Quantitative image contrast enhancement in time-gated transillumination of scattering media

David Sedarsky,[1,*] Edouard Berrocal,[1] and Mark Linne[2]

[1]*Department of Physics, Lund University, Lund, Sweden*
[2]*Department of Applied Mechanics, Chalmers University, Gothenburg, Sweden*
[*]*David.Sedarsky@forbrf.lth.se*

Abstract: Experimental work in turbid media has shown that trans-illumination images can be significantly improved by limiting light collection to a subset of photons which are minimally distorted by scattering. The literature details numerous schemes (commonly termed ballistic imaging), most often based on time-gating and/or spatially filtering the detected light. However, due to the complex nature of the detected signal, analysis of this optical filtering process has been heretofore limited to qualitative comparisons of image results. In this article we present the implementation of a complete system model for the simulation of light propagation, including both the scattering medium and all stages of the optical train. Validation data from ballistic imaging (BI) measurements of monodisperse scatterers with diameter, d = 0.7 μm, at optical depths 5, 10, and 14, are compared with model results, showing excellent agreement. In addition, the validated model is subsequently applied to a modified time-gated optical system to probe the comparative performance of the BI system used in validation and the modified BI system. This instrument comparison examines scatterers with diameters of 0.7 and 15 μm at optical depths 10 and 14, and highlights the benefits of each system design for these specific scattering conditions. These results show that the modified optics configuration is more suitable for particles which are much larger than the incident wavelength, $d >> \lambda$, while the configuration employed in the validation system provides a better contrast for particle diameters on the order of the wavelength, $d \sim\lambda$, where the scattering process exhibits a more homogeneous phase function. The insights and predictions made available by the full numerical model are important for the design of optimized imaging systems suited to specific turbid media, and make possible the quantitative understanding of both the effects of light propagation in the measurement and the performance of the complete imaging system.

OCIS codes: (290.4020) Mie Theory; (290.4210) Multiple Scattering; (290.7050) Turbid Media.

References and links

1. J. C. Hebden, S. R. Arridge, and D. T. Delpy, "Optical imaging in medicine: I. Experimental techniques," Phys. Med. Biol. **42**(5), 825–840 (1997).
2. C. Dunsby and P. M. W. French, "Techniques for depth-resolved imaging through turbid media including coherence-gated imaging," J. Phys. D **36**(14), R207–R227 (2003).
3. R. R. Alfano, S. G. Demos, and S. K. Gayen, "Advances in optical imaging of biomedical media," Ann. N. Y. Acad. Sci. **820**(1 Imaging Brain), 248–271 (1997).
4. W. F. Cheong, S. A. Prahl, and A. J. Welch, "A review of the optical properties of biological tissues," IEEE J. Quantum Electron. **26**(12), 2166–2185 (1990).
5. J. M. Schmitt and G. Kumar, "Optical scattering properties of soft tissue: a discrete particle model," Appl. Opt. **37**(13), 2788–2797 (1998).
6. L. V. Wang and H. Wu, *Biomedical Optics: Principles and Imaging* (Wiley, Hoboken, NJ, 2007).
7. K. M. Yoo and R. R. Alfano, "Time-resolved coherent and incoherent components of forward light scattering in random media," Opt. Lett. **15**(6), 320–322 (1990).

#137309 - $15.00 USD Received 2 Nov 2010; revised 21 Dec 2010; accepted 21 Dec 2010; published 18 Jan 2011

8. L. Wang, P. P. Ho, C. Liu, G. Zhang, and R. R. Alfano, "Ballistic 2-d imaging through scattering walls using an ultrafast optical Kerr gate," Science **253**(5021), 769–771 (1991).
9. G. E. Anderson, F. Liu, and R. R. Alfano, "Microscope imaging through highly scattering media," Opt. Lett. **19**(13), 981–983 (1994).
10. Q. Z. Wang, X. Liang, L. Wang, P. P. Ho, and R. R. Alfano, "Fourier spatial filter acts as a temporal gate for light propagating through a turbid medium," Opt. Lett. **20**(13), 1498–1500 (1995).
11. H. Ramachandran and A. Narayanan, "Two-dimensional imaging through turbid media using a continuous wave light source," Opt. Commun. **154**(5-6), 255–260 (1998).
12. S. Mujumdar and H. Ramachandran, "Imaging through turbid media using polarization modulation: Dependence on scattering anisotropy," Opt. Commun. **241**(1-3), 1–9 (2004).
13. R. Sala and M. C. Richardson, "Optical Kerr effect induced by ultrashort laser pulses," Phys. Rev. A **12**(3), 1036–1047 (1975).
14. M. A. Duguay and A. T. Mattick, "Ultrahigh speed photography of picosecond light pulses and echoes," Appl. Opt. **10**(9), 2162–2170 (1971).
15. L. M. Wang, P. P. Ho, X. Liang, H. Dai, and R. R. Alfano, "Kerr - Fourier imaging of hidden objects in thick turbid media," Opt. Lett. **18**(3), 241–243 (1993).
16. R. R. Alfano, X. Liang, L. Wang, and P. P. Ho, "Time-resolved imaging of translucent droplets in highly scattering turbid media," Science **264**(5167), 1913–1915 (1994).
17. P. A. Galland, X. Liang, and L. Wang, "Time-resolved optical imaging of jet sprays and droplets in highly scattering medium," Proc. Am. Soc. Mech. Eng. **HTD-321,** 585–588, (1995).
18. M. Paciaroni, "Time-gated Ballistic Imaging through scattering media with applications to liquid spray combustion" (Ph.D. Thesis, Colorado School of Mines, 2004).
19. M. Paciaroni and M. Linne, "Single-shot, two-dimensional ballistic imaging through scattering media," Appl. Opt. **43**(26), 5100–5109 (2004).
20. D. Sedarsky, M. Paciaroni, E. Berrocal, P. Petterson, J. Zelina, J. Gord, and M. Linne, "Model validation image data for breakup of a liquid jet in crossflow: part I," Exp. Fluids **49**(2), 391–408 (2010).
21. D. Sedarsky, J. Gord, C. Carter, T. R. Meyer, and M. A. Linne, "Fast-framing ballistic imaging of velocity in an aerated spray," Opt. Lett. **34**(18), 2748–2750 (2009).
22. M. Linne, D. Sedarsky, T. Meyer, J. Gord, and C. Carter, "Ballistic imaging in the near-field of an effervescent spray," Exp. Fluids **49**(4), 911–923 (2010).
23. M. Linne, M. Paciaroni, T. Hall, and T. Parker, "Ballistic imaging of the near field in a diesel spray," Exp. Fluids **40**(6), 836–846 (2006).
24. M. A. Linne, M. Paciaroni, E. Berrocal, and D. Sedarsky, "Ballistic Imaging of Liquid Breakup Processes in Dense Sprays," Proc. Combust. Inst. **32**(2), 2147–2161 (2009).
25. Y. Kuga and A. Ishimaru, "Modulation transfer function and image transmission through randomly distributed spherical particles," J. Opt. Soc. Am. A **2**(12), 2330–2335 (1985).
26. P. Bruscaglioni, P. Donelli, A. Ismaelli, and G. Zaccanti, "Monte Carlo calculations of the modulation transfer function of an optical system operating in a turbid medium," Appl. Opt. **32**(15), 2813–2824 (1993).
27. J. C. Hebden, "Evaluating the spatial resolution performance of a time-resolved optical imaging system," Med. Phys. **19**(4), 1081–1087 (1992).
28. J. C. Hebden and R. A. Kruger, "Transillumination imaging performance: a time-of-flight imaging system," Med. Phys. **17**(3), 351–356 (1990).
29. E. Berrocal, D. L. Sedarsky, M. E. Paciaroni, I. V. Meglinski, and M. A. Linne, "Laser light scattering in turbid media Part I: Experimental and simulated results for the spatial intensity distribution," Opt. Express **15**(17), 10649–10665 (2007).
30. E. Berrocal, D. L. Sedarsky, M. E. Paciaroni, I. V. Meglinski, and M. A. Linne, "Laser light scattering in turbid media Part II: Spatial and temporal analysis of individual scattering orders via Monte Carlo simulation," Opt. Express **17**(16), 13792–13809 (2009).
31. E. Berrocal, "Multiple scattering of light in optical diagnostics of dense sprays and other complex turbid media" (Ph.D. Thesis, Cranfield University, 2006).
32. D. Sedarsky, Ballistic imaging of transient phenomena in turbid media (Ph.D. Thesis, Lund University, 2009).
33. H. Urey, "Spot size, depth-of-focus, and diffraction ring intensity formulas for truncated Gaussian beams," Appl. Opt. **43**(3), 620–625 (2004).
34. M. I. Mishchenko, J. W. Hovenier, and L. D. Travis, *Light Scattering by Nonspherical Particles: Theory, Measurements, and Applications* (Academic Press, London, 2000).
35. D. Watson, N. Hagen, J. Diver, P. Marchand, and M. Chachisvilis, "Elastic light scattering from single cells: orientational dynamics in optical trap," Biophys. J. **87**(2), 1298–1306 (2004).
36. D. Barnhart, "Optica software," *http://www.opticasoftware.com.*
37. Wolfram Research, Inc., Mathematica, Version 7.0, Champaign, IL (2008).
38. E. Hecht, *Optics*, 4th ed. (Addison Wesley Longman Inc., Reading, MA, 2002).

1. Introduction

Optical diagnostics have proven to be crucial to the understanding of a wide range of physical systems where sensitive dynamics require the use of non-intrusive techniques. Optical imaging methods are critical tools applied in fields as diverse as medical imaging, fluid dynamics, combustion, and material science. Increasingly, there is a need for measurements in

#137309 - $15.00 USD Received 2 Nov 2010; revised 21 Dec 2010; accepted 21 Dec 2010; published 18 Jan 2011

adverse environments where interference from multiple scattering and signal attenuation often present significant challenges to conventional optical methods. Transillumination imaging of biological tissue and turbulent two-phase atomizing flows are two important examples.

When light transits a highly scattering medium, most of the photons participate in multiple scattering interactions. Each of these interactions has the potential to change the properties of the transiting photon in a manner which disturbs the fidelity of the optical information that it carries. However, even in extreme scattering environments, a small amount of undisturbed "ballistic" light penetrates the medium. As a result, the transmitted optical signal is made up of a range of photon classes which contribute to the image with different levels of fidelity. This distribution of photon classes extends from ballistic light which exhibits optimal spatial fidelity, to dispersedly scattered light which has been effectively randomized by the turbid environment and appears in the signal as a global background.

The changes in the properties of the source light imparted by interactions with the scattering medium also provide an opportunity to differentiate the multiply-scattered (and therefore less desirable) light from the undisturbed portions of the optical signal. In advanced transillumination optical techniques, image distortion caused by intense scattering is mitigated by constraining the character of the light which is allowed to contribute to the detected intensity. The detected signal is typically filtered by exploiting the temporal, spatial, polarization, and coherence signature of the transmitted light [1–3].

Over the past three decades, a large amount of interest has been shown in the understanding of photon transit through highly scattering media, with much of the early work focusing on near-infrared (NIR) imaging for the characterization of biomedical tissues. Strong interest in this topic is motivated by the possibility of replacing X-ray diagnostics, which utilize harmful ionizing radiation, with NIR radiation diagnostics which are not harmful to the patient. In addition, the absorption and scattering behavior of some tissues offer the possibility for imaging biological function as well as structure. However, as the scattering coefficient of most soft tissues is greater than 10 mm^{-1} in the range of NIR radiation [4,5], the transmitted signal is quickly dominated by multiple light scattering at depths on the order of 1 mm, posing severe limits to both quantitative measurements and qualitative imaging. A variety of optical techniques have been explored to overcome these issues [6].

A number of methods have shown that transillumination images can be significantly improved by limiting light collection to a subset of photons which are minimally distorted by scattering. This approach is commonly known as "ballistic imaging," after the terms first used by Alfano *et al.* to describe light transiting turbid media [7,8]. The most straightforward approach consists in spatial filtering the transmitted light, in order to preferentially select photons based on their direction of propagation [9,10]. This spatial filtering approach is often employed with polarization filtering; see for example the work by Ramachandran *et al.* [11,12]. In addition to spatial and polarization filtering, it is often useful to temporally limit the detected light signal. However, significant improvements using time-gating generally require short gate times, on the order of a few picoseconds. In practice, most systems that take advantage of time-gating to mitigate scattered light are based on the use of the Optical Kerr Effect (OKE) [13].

The first OKE time-gated images were published in 1971 by Duguay and Mattick, using a side-scatter collection geometry and achieving a 10 ps exposure, to image a light pulse propagating through a cuvette [14]. Nearly 20 years later, Wang *et al.* presented OKE time-gated transillumination images through human breast tissue, chicken breast tissue, and a water suspension of polystyrene particles with scattering coefficients up to 21.7 mm^{-1}, utilizing improved laser light sources, optics, and CCD cameras to yield sub-millimeter spatial resolution [8,15]. Alfano *et al.* reported the application of a similar time-gated system to observe water droplets in a milky solution [16], and the first BI results applied to sprays for drop-sizing were reported by Galland *et al.* [17]. In 2004, Paciaroni *et al.* adapted the system of Wang *et al.* to image an optically dense transient spray, obtaining 20 μm resolution single-shot images of an atomizing water spray [18,19].

#137309 - $15.00 USD Received 2 Nov 2010; revised 21 Dec 2010; accepted 21 Dec 2010; published 18 Jan 2011

The application of BI for dense spray diagnostics has generated a renewed interest in the process of photon transit through scattering media, motivated by the possibility to observe multiphase fluid dynamics in spray regions, where substantial questions remain concerning liquid breakup and mixing processes. These efforts are related to and inspired by earlier work, particularly the OKE time-gated imaging of Alfano, *et al.* at CUNY [3,15]. However, the sensitivity and transient nature of sprays give rise to a different set of challenges, and present scattering conditions which differ substantially from biological tissues. Effective diagnostics for sprays dictate a need for resolution at a variety of spatial and temporal scales, and, in general, require that all spatial information is captured within a single, short exposure. To date, the technique has been applied to study a variety of sprays, including jets in cross-flow [20], effervescent sprays [21,22], and high-pressure diesel injectors [23]. Recent progress in BI spray diagnostics was reviewed by Linne *et al.* in 2009 [24].

In addition to numerous qualitative demonstrations of image contrast improvement by limiting light collection, a number of quantitative efforts have been put forward to understand the scattered light signal and its possible effects on image contrast. Work by Kuga and Ishimaru examined the collection of scattered light by a single lens, estimating the modulation transfer function (MTF) for various solutions of spherical particles at optical depths ranging from 0 to 15 [25]. A similar investigation based on a numerical Monte Carlo approach, was applied by Bruscaglioni *et al.* at optical depths ranging from 0 to 7 [26], corresponding to the intermediate scattering regime. Scattering from somewhat larger optical depths, corresponding to the multiple scattering regime, were examined by Hebden *et al.*, reporting both experimental results [27] and numerical analysis [28] for image contrast improvements by time-gating. More recent work by Berrocal *et al.* examines aspects of the spatial [29] and temporal spreading of scattered light using Monte Carlo simulations to infer the effects of scattering on image contrast [30].

Despite these early research efforts, assessment of the effectiveness of optical filtering methods has been mainly limited to qualitative comparisons of individual measurements, due to the labor intensive nature of experimental system characterization. In addition, detailed insight into the light filtering process, which is a function of the interdependent properties of the source, scattering medium, and system optics, is not easily made available through experiment. A full understanding of light propagation within a given scattering medium, including the effects of the system optics, is required to quantitatively understand how the system functions, and how it can be optimized for a specific application. Of particular interest is the idea that one can develop techniques which enable conventional diagnostics to overcome the limitations imposed by severe scattering such that they could be extended to more challenging optical conditions. To reach that point requires methods which enable a firm understanding of the aggregate effects of scattering and light transmission in a turbid environment.

This work presents a numerical model which can be applied to light scattering in a complete optical system, thus providing a tool for detailed quantitative analysis of light propagation through a scattering medium and at all stages of the optical train. This enables analysis and optimization of the full imaging system, and a direct means of calculating and understanding the image contrast enhancement produced by the instrument. Results from this model are validated by comparison with measurements for a time-gated ballistic imaging system applied to monodisperse 0.7 μm scatterers at three optical depths. Finally, the model is applied to compare two different optical arrangements, allowing the effects of the optics on the resulting image contrast to be quantitatively examined through simulation.

2. System model implementation

The system model presented here is a set of programs that work together to define a light source, a scattering volume, and instrument optics. For a typical imaging application, an intense short pulse of source light is modeled by numerous “photon packets”, representing groups of photons which follow similar trajectories. This light is transmitted through the scattering volume and optics to form a spatial intensity profile at the detection plane of the

#137309 - $15.00 USD Received 2 Nov 2010; revised 21 Dec 2010; accepted 21 Dec 2010; published 18 Jan 2011

system. Light propagation in the model scattering volume is calculated as the sum of many distinct photon-particle interactions. The photon packets representing the source light are launched and tracked through the scattering volume using a validated Monte Carlo (MC) code designed for light scattering in random inhomogeneous media [29–31]. The information from this MC code is integrated with a custom ray-tracing model which implements spatial, temporal, and polarization filtering of the source light as it traverses the optical train to reach the output plane [32]. This yields a spatial intensity profile, which is subsequently convolved with a Gaussian kernel representing the diffraction limited spot-size [33] of the optical system. This scheme represents a computationally affordable approach (simulations run on an individual desktop machine) for calculating photon trajectories in regions containing a large number density of spherical scatterers and allows the quantitative evaluation of different imaging instruments and light filtering schemes. This provides the opportunity to optimize individual components, identify problems in current systems, and test the feasibility of new measurement objects, light sources, or optical designs.

2.1. Monte-Carlo light scattering

The MC approach used to simulate the scattering volume determines likely values for the physical circumstances of each photon packet as it propagates from the source to its final position. This is accomplished by randomly sampling probability distributions for photon interaction and direction change, which are based on the mean free path in the medium, and an appropriate scattering phase function determined by Lorenz-Mie theory, respectively [31].

The MC method relies on repeated random sampling. Individually, each randomly determined answer represents only a possible answer. Large numbers of randomly sampled values in aggregate, however, begin to portray a realistic picture of the physical system, as represented by the probability distributions. By providing a statistically significant number of samples, light propagation throughout the optical scattering medium can be accurately calculated. This approach provides an approximation to the exact solution of the radiative transfer equation.

It is important to note that the use of the Mie scattering phase functions to represent the scattering medium implicitly restricts accurate simulation to situations where Mie scattering assumptions are valid. Here, we assume that scattering events in the simulation are mutually independent, and the scatterers are approximately spherical, resulting in a phase function which is independent of the orientation of the incoming light.

While it is possible to apply the present model with distributions determined from other phase functions which take into account the effects of aspherical, interfering particles [34,35], the determination of such phase functions is itself an area of active research and frequently involves significant increases in error or computational effort. At present, many applications of the model for understanding and improving optical diagnostics are likely to be better served by utilizing Lorenz-Mie phase functions.

2.2. Ray-tracing through system optics

While a stochastic MC approach is efficient and easily adapted for modeling light propagation in a volume of dense and randomly distributed scatterers, a deterministic ray-tracing approach is more suitable for the simulation of light propagation through a succession of well-defined optical components. For this reason, the system model presented in this article integrates the MC scattering implementation together with a detailed ray-tracing model which is implemented in Rayica and Mathematica code [36,37].

The ray-tracing method used here consists of an array of surfaces, material properties, and interaction behaviors which accurately describe each individual optical component. The pertinent information generated by the MC procedure, including optical path length, time, scattering order, position, direction and polarization for each simulated photon, form the basis for a source ray which can be explicitly traced through the surfaces and material models which make up the complete optical arrangement. Photon packets are filtered based on the time-gating condition and traced through the system optics from the source to the detector.

#137309 - $15.00 USD Received 2 Nov 2010; revised 21 Dec 2010; accepted 21 Dec 2010; published 18 Jan 2011

Here, the light is integrated in the detection plane, yielding a two-dimensional spatial intensity signal which is then convolved with the diffraction-limited spot-size of the system optics, resulting in an accurate representation of the light imaged at the output plane.

This ray-tracing arrangement allows the light information handled by the MC code to be effectively filtered to yield the spatial intensity incident on the detector in a physical imaging system. In addition, the ray-tracing approach further contributes to the utility of the model as an instrument design tool, since existing high-quality models of commercial optics, and ray-tracing optimization methods can be leveraged to refine the instrument response.

3. Model validation against experiment

Previous work by Paciaroni [18] included careful spatial resolution measurements for a BI system where the contrast transfer and point spread functions of the instrument were evaluated experimentally by imaging a test-chart immersed within various suspensions of polystyrene microspheres in water over a range of optical depths. A diagram of this imaging arrangement is shown in Fig. 1. Paciaroni demonstrated that this instrument is capable of single-shot imaging through 0.7 μm scatterers at optical depths as high as 14.

3.1. Experimental setup

Source light for the measurements was provided by a Ti:sapphire regenerative amplifier (Spectra-Physics Spitfire), which produces linearly polarized laser pulses with a peak power of 1 mJ, 80 fs pulse duration, and a center wavelength of 800 nm. The input light crosses the scattering volume and is collected by a lens placed one focal distance from the center of scattering volume. Light gathered by the lens is focused through an optical Kerr effect (OKE) shutter [13], formed by a pair of crossed Glan-Taylor polarizers which bracket a Kerr medium, consisting of a glass cuvette filled with liquid carbon disulfide. The OKE shutter is gated by a switch pulse, which is formed from light split from the image pulse. The resulting 2 ps time-gate was positioned to maximize the first-light signal. Light transmitted by the OKE shutter is subsequently collected by a second lens and directed to a display screen where it is imaged by an EM-CCD camera. Table 1 lists the details for the optical components utilized in this imaging arrangement.

This optical arrangement eliminates a large portion of the forward-scattered source light transmitted through the scattering medium by discriminating photons based on their collimation, polarization, and optical path length. Inadequately collimated light is filtered by the acceptance angle of the collection optics, randomly polarized light is eliminated by the polarization optics (crossed polarizers and the birefringent Kerr medium), and the optical path length of detected light is limited by the time-gating action of the OKE shutter. The time response of the Kerr shutter was investigated in [18] (see Fig. 3(b) below).

Table 1. Ballistic Imaging optical components used in validation measurements

Symbol	Component	Supplier	Part no.	Notes
M1	Mirror	Newport	10d510ER2	$R > 96\%$
M2	Mirror	Edmund Scientific	45597	$R > 99\%$
L1	Achromatic lens	Newport	PAC088	$f_1 = 250$ mm
L2	Achromatic lens	Newport	PAC091	$f_2 = 500$ mm
P1	Glan polarizer	Melles Griot	PTYL-25-670-1064	$CaCO_3$ cube
P2	Glan polarizer	Melles Griot	PTYL-10-670-1064	$CaCO_3$ cube
WP	Retardation plate	Newport	10RP02-XX	½ wave
BS	Beamsplitter	Melles Griot	UT-800-30-45	70% trans.
KC	Cyl. opt. Kerr cell	NSG	T-32	10 mm length

#137309 - $15.00 USD Received 2 Nov 2010; revised 21 Dec 2010; accepted 21 Dec 2010; published 18 Jan 2011

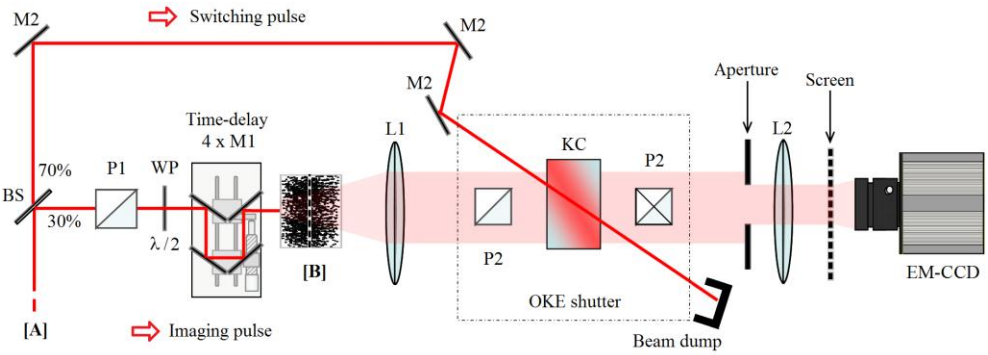

Fig. 1. Experimental arrangement used for ballistic imaging validation measurements: The input pulse [A], centered at 800 nm, with 80 fs pulse width and 1 mJ pulse energy, is divided by a beam-splitter, forming a strong 'switch' pulse and a weaker 'image' pulse. The image pulse is directed through a 10 mm long cuvette [B] containing a water solution of 0.7 μm polystyrene spheres. A test chart is immersed in the center of the cuvette and the transmitted light is subsequently collected and filtered by the lenses and OKE shutter. The OKE shutter (~2 ps) is driven by the switch pulse, which is directed through the Kerr cell containing liquid carbon disulfide. Spatial information from the test chart is transmitted to the screen and recorded by an EM-CCD camera. Details for each optical component are listed in Table 1.

3.2. Model arrangement for validation

The system model presented in this work was applied to the optical arrangement and conditions used by Paciaroni in her experimental system characterization [18,19], providing a convenient validation control for the numerical system model. In the simulation, the refractive indices of the surrounding medium (distilled water) and of the scatterers (polystyrene spheres) were set to 1.33 and 1.58 respectively. The incident illumination was assumed to be monochromatic, with a wavelength, λ = 800 nm. The entire scattering volume was assumed to be non-absorbing such that the scattering coefficient μ_s is equal to the extinction coefficient μ_e. Three different scattering media were examined in the experiments and computations, consisting of monodisperse microspheres with a diameter, d = 0.7 μm, at optical depths of *OD* = 5, 10 and 14, corresponding to extinction coefficients, μ_e = 0.5, 1.0 and 1.4 mm^{-1} respectively. The presence of the resolution test chart was simulated at the center of the 10 mm long scattering volume by spatially modulating the light crossing the object plane with bar pattern (square wave) at a given frequency. For each scattering medium, simulations were performed over spatial frequencies ranging from 1 to 50 lp/mm. The transmitted photons within the detection angle of the collecting lens L1 were traced through the successive optics to form an image of a 5 × 5 mm square-wave pattern (representing the test chart) on a 512 × 512 detector array. An illustration of the complete modeling optical setup is shown in Fig. 2.

By arranging the light collection lens L1 at 1*f*, a projection imaging system efficiently gathers collimated and nearly collimated photons that traverse the object plane. This contributes to the spatial filtering effect such that the collection of uncollimated light scattered behind the object is reduced, while the collection of well-collimated light remains unaffected. This is similar to the arrangement of a condenser lens used to project light from a small source into an optical system. Note that this optical configuration was originally adapted from the "Kerr-Fourier" imaging set-up presented in [15]. While this arrangement maximizes the light intensity collected from the center of the focal plane of the collection lens, it does not form an image in the classical sense. The collected signal represents a projection of this object plane. As such, the quality of the spatial intensity at the detector is heavily influenced by the collimation and intensity of the source light as it reaches the object plane.

#137309 - $15.00 USD Received 2 Nov 2010; revised 21 Dec 2010; accepted 21 Dec 2010; published 18 Jan 2011

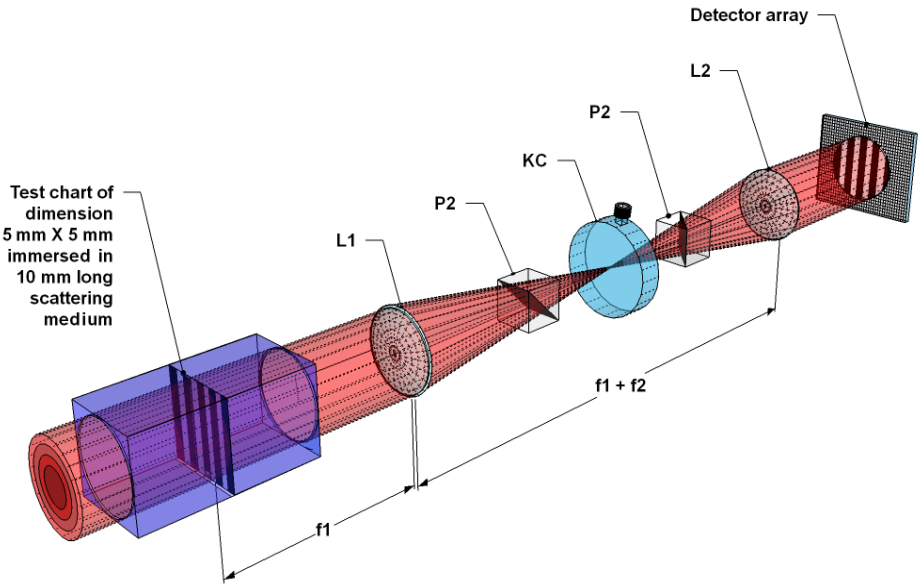

Fig. 2. Optical arrangement for the validation of the model with experimental results: light transmitted from the scattering volume (calculated by MC simulation) is collected by a lens placed at a distance, 1*f*, from the object plane and is projected to the detector face after crossing the OKE shutter. This optical arrangement is referred to as the *"projection"* system in the text. Note that the optical response of each optical component — related to the experimental set-up shown in Fig. 1 and detailed in Table 1 — is accurately simulated by the ray-tracing code.

It is important to point out that the model is fully predictive, there are no adjustments made to match measurements. It's also necessary to mention that the temporal profile of the source light was modeled as a Dirac delta function in the simulation, while the laser pulses used in the experiment were produced by an amplified mode-locked laser system, which produces pulse durations of ~80-100 fs, as indicated in Fig. 3(a). Furthermore, a constant time-gate with a duration of 2 ps, was assumed in the simulation whereas the OKE time-gate used in the experimental work exhibits a dynamic response based on the relaxation characteristics of liquid carbon disulfide, as shown in Fig. 3(b).

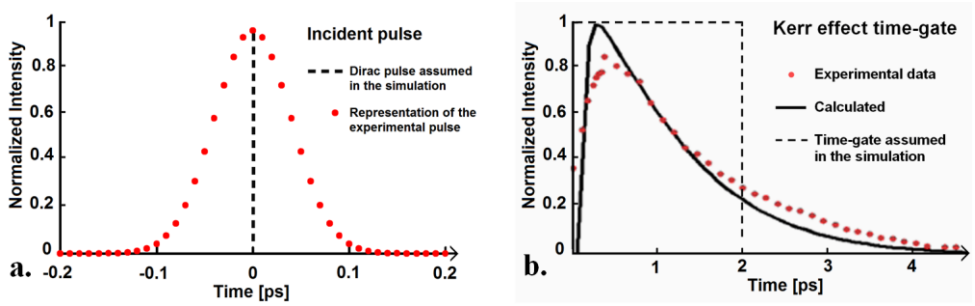

Fig. 3. (a) Representation of the temporal characteristics of the experimental (dots) and simulated pulses (dashed line). (b) Temporal characteristics of the CS_2 OKE shutter measured experimentally (dots) [13] together with the 2ps constant shutter assumed in the simulation (dashed line).

The use of these approximations reduces the accuracy of the numerical model to some degree, as the effects of the finite pulse width and the efficiency of the time-gate are ignored in the simulation. This represents a minor source of error in the model, provided that the temporal width of the source is small compared to the transmitted pulse and the efficiency of the OKE time-gate is high and well-behaved. It is feasible to include these effects in the

#137309 - $15.00 USD Received 2 Nov 2010; revised 21 Dec 2010; accepted 21 Dec 2010; published 18 Jan 2011

modeling effort. However, in the opinion of the authors, the benefits of a simpler model, in terms of understanding aggregate scattering effects and the efficacy the collection optics, outweigh the disadvantage of this small loss in accuracy.

3.3. Image contrast evaluation: Comparison between experiment and simulation

An essential aspect of an optical system is its ability to transmit spatial information. The relevant parameter for evaluating performance in this respect is the visibility, or image contrast [38]. Imaging a square-wave test pattern provides a convenient method to estimate the spatial response of the optical system at a single spatial frequency. For the fundamental spatial frequency of the square-wave pattern, the contrast of the image, *C*, is defined as:

$$C = \frac{I_{max} - I_{min}}{I_{min} + I_{max}} \tag{1}$$

where I_{min} and I_{max} are the respective minimum and maximum intensities of the imaged square-wave pattern. By modulating the spatial frequency of the imaged square-wave pattern within each scattering medium (*OD* = 5, 10 and 14) and applying the system model to calculate the instrument response, a series of simulations can be used sample the contrast transfer function (CTF) of the modeled instrument, yielding a quantitative metric for its performance as an imaging system. In addition, the point-spread function, representing the spatial distribution of irradiance produced by the instrument in response to a point source, can be calculated as the normalized modulus of the Fourier transform of the CTF. Figure 4(a) shows the simulated CTF generated by this procedure for the validation optics, compared with the experimental CTF given by [18]. Figure 4(b) shows the corresponding PSF comparison for the system model and measurement results.

The simulated and measured values given in Fig. 4 show good agreement and similar trends are obtained over the entire frequency range. Note that this model is not "tuned" to force agreement with experiment; the model has no adjustments. The agreement with experiment thus confirms that this is a predictive model within the range of validity of the assumptions that were applied.

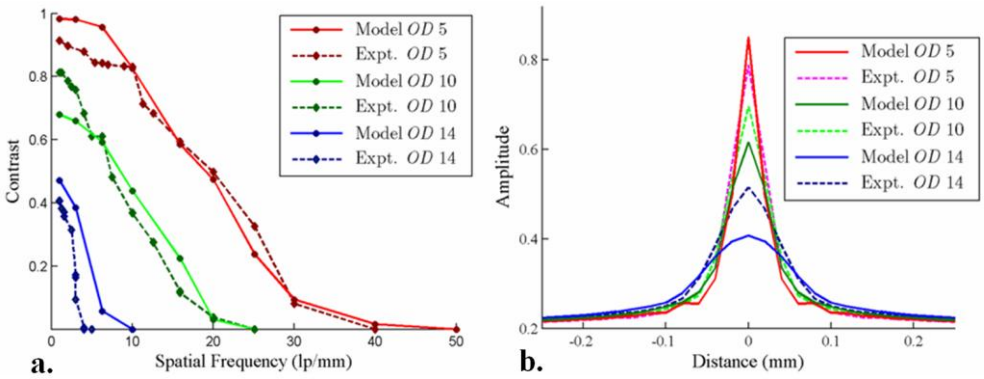

Fig. 4. Experiment and simulation comparison for the Contrast Transfer Function (a) and the Point-Spread Function (b) for the optical arrangement diagramed in Fig. 1 and Fig. 2. These validation results examine the response of this time-gated (~2ps) imaging instrument through a scattering volume containing 0.7 μm polystyrene spheres at optical depths of 5, 10 and 14.

4. Comparison between two Ballistic Imaging optical systems

The validated model can be utilized to investigate different scattering conditions or system geometries, or to compare the effects of different light collection arrangements. To this end, the optical arrangement used in the validation experiments discussed in the previous section is now compared with a modified light collection setup. For convenience, we refer to the

#137309 - $15.00 USD Received 2 Nov 2010; revised 21 Dec 2010; accepted 21 Dec 2010; published 18 Jan 2011

validation setup as the "*projection"* system, and the modified setup as the *"one-to-one imaging"* system.

4.1. Description of the simulation

The aim of this optical system comparison is to quantitatively explore the effects of two different ballistic imaging instruments without radically changing the optical layout or introducing significant changes from new optical components. Hence, the design choices for these systems were dictated first by the constraint to use similar optics, and second with the aim of maximizing image contrast performance. The model arrangement of the first system is fully described in subsection 3.2 and illustrated in Fig. 2. The model arrangement of the second system is depicted in Fig. 5. The major differences between the two systems arise as a result of the placement of the first light collection lens, placed at 1*f* from the object plane for the *projection* system and 2*f* for the *one-to-one imaging* system.

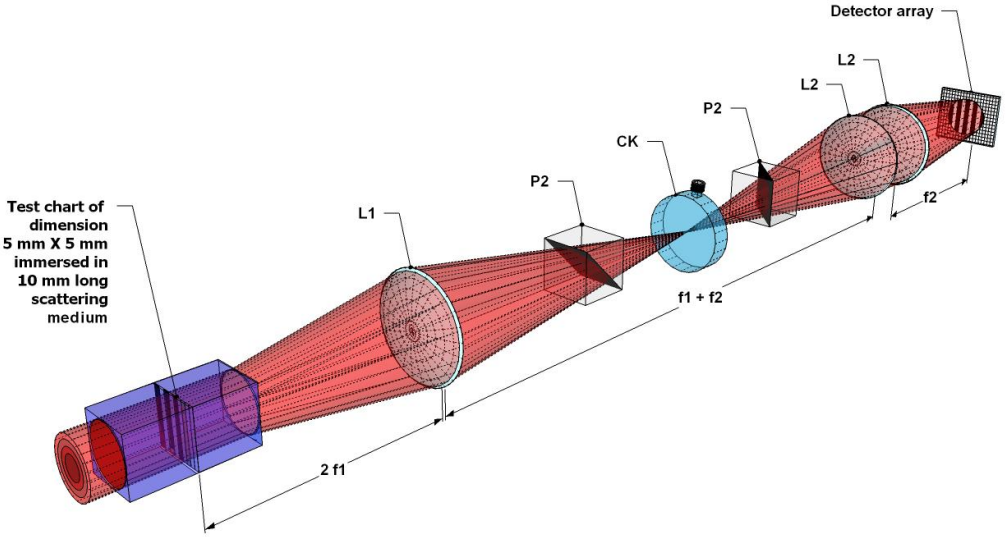

Fig. 5. Optical arrangement for the *"One-to-one imaging"* system: light transmitted from the scattering volume (calculated by MC simulation) is collected by a lens placed at a distance, 2*f*, from the object plane. This configuration forms an image that is relayed to the detector face at unit magnification. A second lens, L2, is used here to form an image of the 5 x 5 mm test chart at a convenient distance and collected by a 512 x 512 detector array. Note that the optical response of each optical component — detailed in Table 1 — is accurately simulated by the Ray-tracing code.

The light collected at 2*f* by the lens L1 forms an image with a conjugate relation to the object plane, which is then relayed by the optics following the collection lens, forming an image at unit magnification on the face of the detector. This collection scheme preserves high frequency spatial information, but reduces the light contributed by each point within the object plane, since the irradiance filling the aperture of the light collection lens decreases according to the inverse square of the distance from the object. Note that the length of the optical train as well as the respective apertures of the components spatially filter the collected light, excluding the photons scattered into higher angles which propagate off axis.

#137309 - $15.00 USD Received 2 Nov 2010; revised 21 Dec 2010; accepted 21 Dec 2010; published 18 Jan 2011

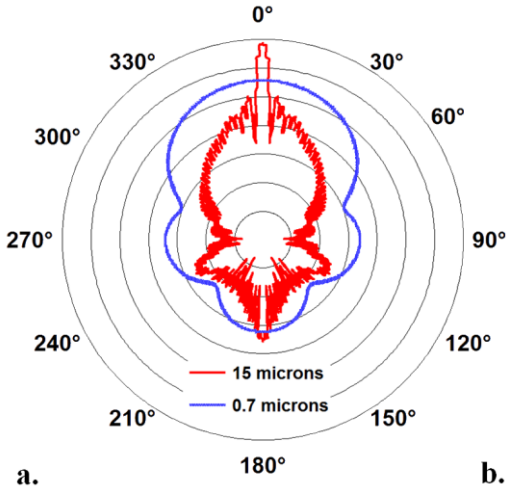

b.

Particle size	$d = 0.7\ \mu$m	$d = 15\ \mu$m
Wavelength: λ [nm]	800	800
Refractive index particles: n_p	1.58+0.0i	1.58+0.0i
Refractive index medium: n_m	1.33+0.0i	1.33+0.0i
Anisotropy factor: g	0.845	0.920
Extinction cross-section: σ_e [mm^2]	3.390 10^{-7}	4.006 10^{-4}
Number density at *OD* 10: N [#/mm^3]	2.950 10^{6}	2496
Number density at *OD* 14: N [#/mm^3]	4.130 10^{6}	3494
Scattering parameter: $X = (\pi \cdot d / \lambda)$	2.75	58.9

Fig. 6. (a) Polar plot - logarithmic scale - of the angular Lorenz-Mie scattering phase functions for the two different sizes of polystyrene microspheres. The phase function for 0.7 μm (blue line) with broad-lobed, relative homogeneous angular distribution is shown superimposed on the 15 μm phase function (red line) which exhibits a strong forward scattering peak. Note that the phase functions shown here are circularly symmetric about the central (vertical) axis. The corresponding optical characteristics of the scattering particles and medium are shown in (b).

In a manner analogous to the simulations presented in the previous section, results for the two-system comparison were generated by modeling a 10 mm long scattering medium of monodisperse polystyrene spheres immersed in water. However, the analysis is confined to a single spatial frequency (1 lp/mm) and the effects of time-gating from 0 to 4 ps are investigated in detail. A selection of conditions were examined by considering 0.7 and 15 μm particles, at optical depths of 10 and 14. The scattering phase functions of the particles are shown in Fig. 6(a) together with their related optical properties in Fig. 6(b).

4.2. System performance comparison for the 0.7 µm particles

The optical responses for the 0.7 μm scatterers, at *OD* 10 and *OD* 14, are shown for the *projection* and *one-to-one imaging* configurations in the movies linked to Fig. 7(a) and 7(b) respectively. The image contrast and detected signal intensity from these data are presented as a function of time-gating in Fig. 8, providing a quantitative comparison between the two optical arrangements. Note that the light intensity shown is normalized to the respective total detected intensity (when no time-gate is applied) for each system.

At *OD* 10, the bar chart test pattern is discernible with both optical arrangements even with no time-gating, as indicated by the horizontal line in Fig. 8(a) and 8(b). Here, from the standpoint of image contrast, it is clear that the *projection* system outperforms the *one-to-one imaging* system over the entire range of the time-gating.

#137309 - $15.00 USD Received 2 Nov 2010; revised 21 Dec 2010; accepted 21 Dec 2010; published 18 Jan 2011

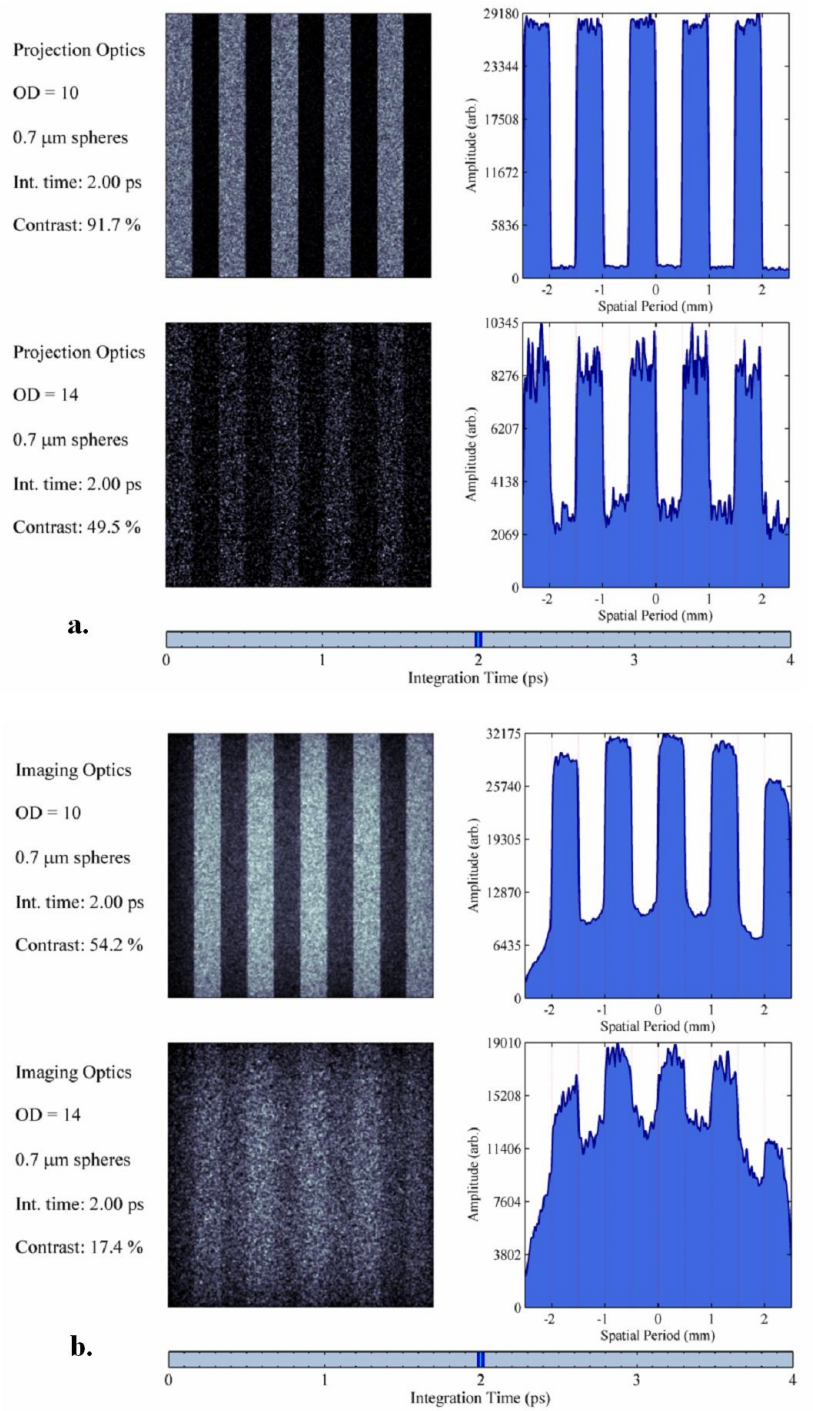

Fig. 7. Calculated images and contrast for 0.7 μm scatterers: subfigure (a) and linked media (Media 1) show the *Projection* system; subfigure (b) and linked media (Media 2) show the *one-to-one imaging* system. Results are shown together with the corresponding plots of 1-D (summed) intensity vs. spatial period for the conditions listed on the left. The linked media files show these results over integration times from 0 to 4 ps.

#137309 - $15.00 USD Received 2 Nov 2010; revised 21 Dec 2010; accepted 21 Dec 2010; published 18 Jan 2011

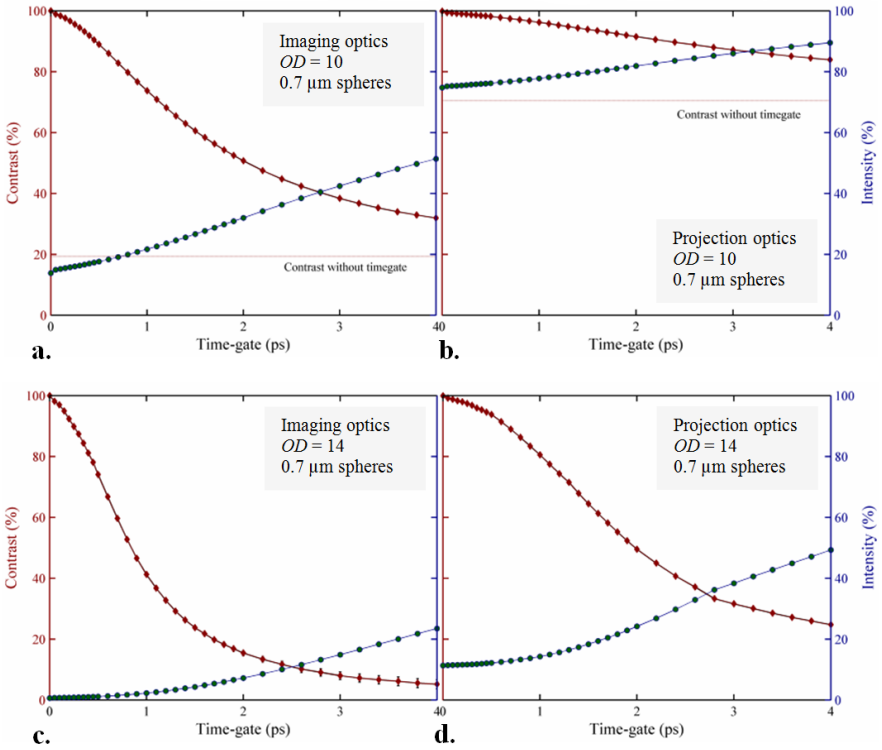

Fig. 8. Simulation results for *one-to-one imaging* and *projection* optical arrangements, for 0.7 µm scatterers, at *OD* = 10 and 14. Note that for the lower *OD* conditions shown in (a) and (b) the test pattern is discernible even when light collection is not filtered by the time gate.

The movies linked to Figs. 7(a) and 7(b) reveal the dynamics of the time-resolved imaging performance for each system and highlight differences between the *projection* results (a) and *one-to-one imaging* results (b). Note that the level of the collected intensity is at 2 ps is higher in (b) than in (a) for both *OD*'s. The average profile of the summed (1-D) spatial intensity is flat in (a), but a rounded profile which is higher in the center and diminished near the edges is apparent in (b).

Examining the results shown in Fig. 8 together with the scattering phase function shown in Fig. 6(a), it is apparent that the relatively homogeneous scattering exhibited by the 0.7 μm scatterers prevents a significant portion of the scattered light from propagating to the collection lens. Light penetrates the medium less effectively, since scattering interactions are very likely to result in large direction changes, but light that does penetrate remains well-collimated. This contributes to a stronger signal-to-noise ratio (SNR) for the *projection* system versus the *one-to-one imaging* system. In short, the light incident on the *projection* optics due to the placement of the first lens and the action of the 0.7 µm scatterers results in a large relative signal contribution from well-collimated photons.

The *projection* system collects line-of-sight integrated spatial information from the scattering volume corresponding to the object plane; the signal relies heavily on relatively undisturbed ballistic and scattered light transiting the medium. This is apparent in the video linked from Fig. 7(a), showing 2-D and summed 1-D views of the spatial intensity results. A strong contrast is discernible over the entire time-gating range; however, most of the signal contributing to image contrast arrives at the detector within the first ~1.5 ps and contrast steadily decreases as the detection time increases. The noise appears as level background, uniformly distributed over the image, and the edges of the bar pattern retain their shape even as contrast decreases.

#137309 - $15.00 USD Received 2 Nov 2010; revised 21 Dec 2010; accepted 21 Dec 2010; published 18 Jan 2011

The *one-to-one imaging* system efficiently collects light scattered within the object plane, allowing signal contributions from both collimated and uncollimated light. Observing the spatial intensity results in the video linked to Fig. 7(b), one can see that the bar pattern is well-defined for very short gate times, but is gradually distorted by diffusely scattered light collected by the one-to-one imaging optics. Here, the noise is initially most apparent near the edges of the bar pattern and spreads outward from each bar as photons with later arrival times are allowed to contribute to the image. The reduced fidelity of the signal is also manifested in the shape of the summed 1-D intensity peaks, which take on a rounded appearance. This is indicative of the spatial distortion produced by the scattering volume, which has a greater effect on the higher spatial frequency components of the square-wave pattern.

For these scattering conditions, the *projection* system outperforms the *one-to-one imaging* system predominately for two reasons. First, since the scattering is relatively homogeneous, interactions in the medium direct much of the source light in other directions. This increases the effectiveness of the spatial filtering of the *projection* light collection arrangement because it favors collimated light. Second, the *one-to-one imaging* arrangement collects uncollimated (scattered) light appearing in the object plane; the fidelity of this signal suffers directly from the statistically large angular distortions imparted by the 0.7 μm scattering medium.

4.3 System performance comparison for the 15 μm particles

The optical responses for the 15 μm scatterers, at *OD* 10 and *OD* 14, are shown for the *projection* and *one-to-one imaging* configurations in the movies linked to Fig. 9(a) and 9(b) respectively. From these movies, the image contrast and detected signal intensity are presented as a function of time-gating in Fig. 10. This figure provides a quantitative comparison between the two optical arrangements. Note that the light intensity shown is normalized to the respective total detected intensity (when no time-gate is applied) for each system.

At *OD* 10, the bar chart test pattern is faintly visible with the *one-to-one imaging* arrangement even with no time-gating, as indicated by the horizontal line in Fig. 10(a). Here it is important to note that the time scales for the *projection* results, shown in Fig. 10(b) and 10(d) are given in femtoseconds, and that the test pattern is completely indiscernible from the background intensity using the *projection* arrangement for all but the shortest simulated gate-times. Here, the *one-to-one imaging* system outperforms the *projection* system, in contrast to the scattering results in the preceding section.

Examining the phase functions shown in Fig. 6(a), one can see the angular scattering distribution exhibited by the 15 μm scatterers differs significantly from the 0.7 μm scatterers. As a consequence, the aggregate effects of light scattering through a distribution of 15 μm scatterers result in an optical signal which propagates in a manner unlike that produced by the previous conditions. Effects from the forward-scattering peak (near zero degrees) of the 15 μm phase function, contribute a significant number of 'quasi-collimated' photons to the forward-propagating light signal; photons which have been slightly perturbed by scattering but remain within the collection angle of the optical system. As a result, the bulk of the forward-propagating light is no longer strictly collimated as it transits the medium, but instead adapts a level of collimation balanced by the effects of the collection optics, the phase function, and the geometry of the medium.

For the *projection* system, the character of this forward-propagating light reduces the effectiveness of the spatial filtering, allowing significant amounts of distorted forward-scattered light to contribute to the collected spatial intensity. This results in very low SNR for all but the shortest time-gating conditions for the *OD*'s examined here. In addition, because the optics project light forward without forming an image at the detection plane, light scattered from the object plane does not form a positive signal contribution.

#137309 - $15.00 USD Received 2 Nov 2010; revised 21 Dec 2010; accepted 21 Dec 2010; published 18 Jan 2011

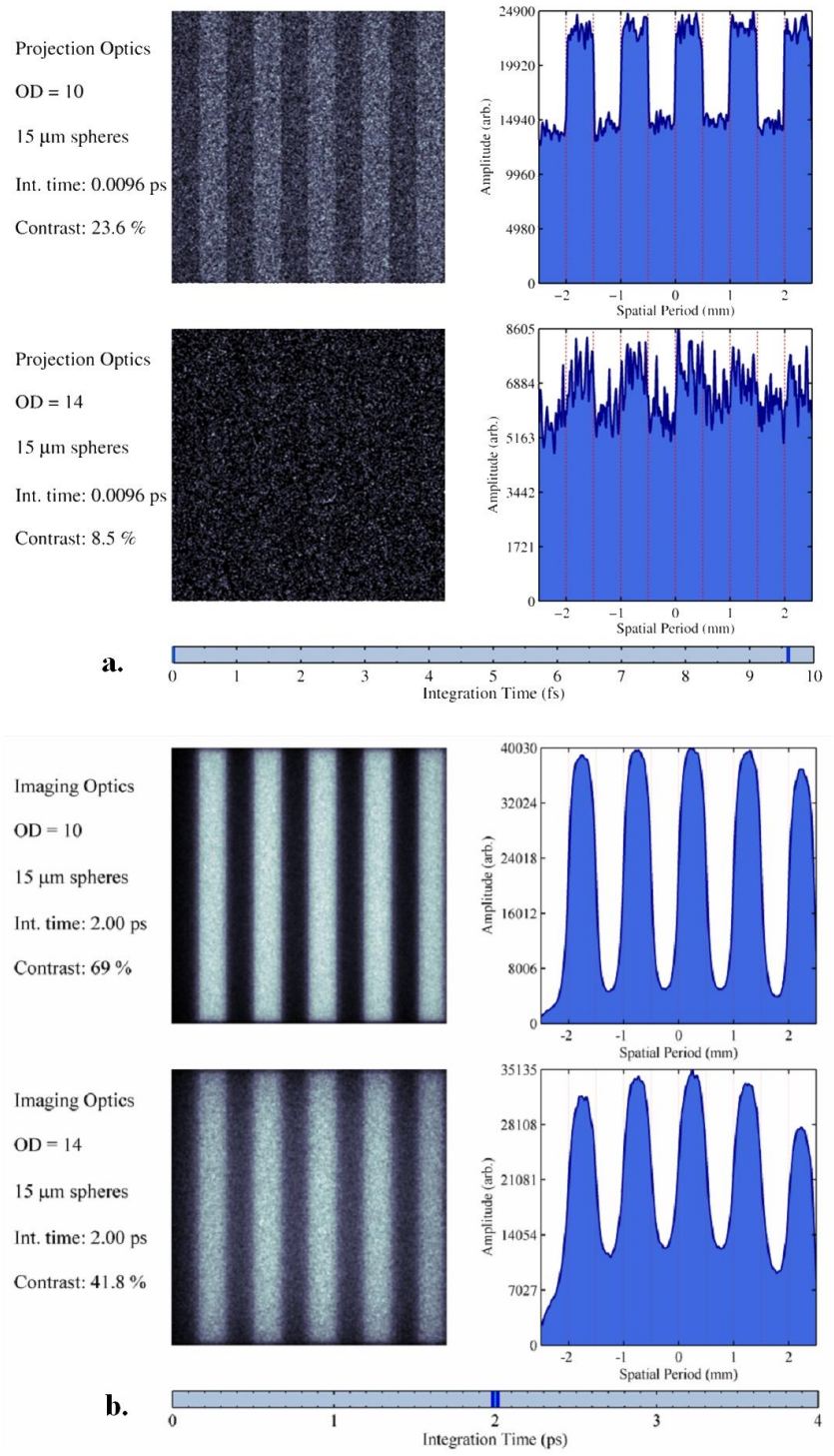

Fig. 9. Calculated images and contrast for 15 μm scatterers: subfigure (a) and linked media (Media 3) show the *Projection* system; subfigure (b) and linked media (Media 4) show the *one-to-one imaging* system. Results are shown together with the corresponding plots of 1-D

#137309 - $15.00 USD Received 2 Nov 2010; revised 21 Dec 2010; accepted 21 Dec 2010; published 18 Jan 2011

(summed) intensity vs. spatial period for the conditions listed on the left. The linked media files show these results over integration times from 0 to 4 ps.

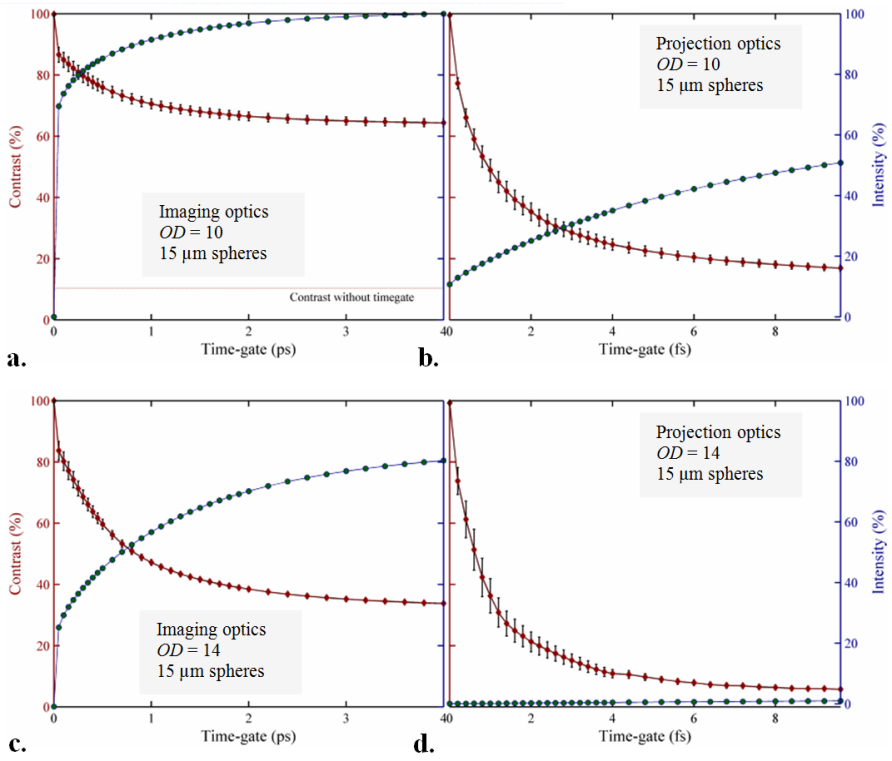

Fig. 10. Simulation results for *one-to-one imaging* and *projection* optical arrangements for 15 μm scatterers, at *OD* = 10 and 14. Note that the time scales in (b) and (d) are given in femtoseconds.

The *one-to-one imaging* system, however, is better suited for discriminating high-quality imaging light from the 15 μm scattering signal, as evidenced by the results shown in Figs. 10(a) and 10(c). Here, the placement of the first light collection lens further from the object plane decreases the effective collection acceptance angle, slightly reducing contributions from off-axis light. More importantly, since the *one-to-one* optics collect and focus light from the object plane to form an image at the detector, much of the light scattered within the object plane contributes positively to the spatial intensity signal. For these results, the highly forward nature of the scattering from the 15 μm particles allows more source light to illuminate the object plane, increasing this signal contribution. The fidelity of this signal, however, is degraded to some extent by the small angular perturbations imparted by scattering in the medium. The reduced fidelity of the signal as a result of these perturbations is apparent in the shape of the summed 1-D intensity peaks (see, e.g. Figure 9(b)). Here the 1-D intensity appears almost sinusoidal, indicating that spatial distortion from the scattering medium disrupts most of the higher frequency components of the square-wave spatial intensity.

4.4. Implications for imaging in turbid media

With the advent of the model introduced in this work, we have demonstrated that detailed quantitative analysis of imaging in turbid media is now possible. It is clear from the results shown in the preceding subsections that scattering conditions and light detection arrangements which appear to be very similar can produce non-intuitive effects on imaging measurements do to the competing interactions of aggregate scattering effects, light collection, and detection

#137309 - $15.00 USD Received 2 Nov 2010; revised 21 Dec 2010; accepted 21 Dec 2010; published 18 Jan 2011

limits. This underscores the need for proper understanding of the complete system to improve the application of BI diagnostics.

More complex optical arrangements in medical imaging applications can take advantage of this full-system analysis for optimization and a deeper understanding of the optical signal. However, these benefits are likely to be incremental advances. The qualitative understanding of light scattering in most tissues of interest is well-established in the literature. In addition, the nature of medical imaging problem often lends itself to raster-scanning single-point techniques, where averaging and other signal adjustments make detailed time-resolved understanding of a single transmitted pulse less critical.

This level of detailed understanding is of particular importance with regard to the application of BI diagnostics in dense transient sprays, which can exhibit a diverse range of scattering conditions. Hence, there is a risk that present applications targeting sprays are misled by the trends and understanding established by years of qualitative medical imaging development, which is valid under scattering conditions specific to tissue imaging. Some indications for imaging in spray conditions are apparent from the brief analysis given in this paper, however, more widespread application of the model covering a range of spray conditions is necessary to establish reliable general prescriptions for the application of BI to different sprays.

5. Conclusions

Light collected in forward-scatter can provide access to spatial information which is otherwise obscured by signal loss and distortion in highly scattering environments. However, to realize the full potential of scattered light imaging diagnostics requires an understanding of the optical signal specific to the scattering conditions under study. The system simulation model discussed and validated in this work provides an essential tool for quantitative understanding of the scattered light signal for a complete optical system, allowing proper design and optimization of imaging systems suited to acquiring spatially resolved information in turbid media.

The application of the model presented in section 4 illustrates how the aggregate effects of light scattering can produce significant variations in the optical signal, such that an imaging system optimized for one condition may be poorly suited for other scattering conditions. Although some trends in the aggregate signal can be inferred by examining the phase function appropriate to scattering in the medium, conclusions regarding the effect on image contrast drawn on this basis are especially prone to error, due to the complex interaction of the light collection optics, aggregate scattering effects, and the system geometry.

Both of the optical systems examined in this work present distinct advantages for collecting spatial information from turbid environments. The image contrast analysis derived from the system model in each case provides insight into the effects of light collection for the chosen scattering conditions. With proper discretion regarding changes to the scattering geometry, collection optics, and the scattering phase function, these insights can be applied as a rough prescription for extracting image information from a turbid scattering volume.

If the forward-scatter signal is well-collimated and adequate for imaging detection limits, an instrument similar to the *projection* system, which reduces scattered-light collection can provide high image contrast, while an approach similar to the *one-to-one imaging* system will generally produce lower contrast due to contributions from distorted light from the object plane.

If the forward-scatter signal is not strictly collimated, but includes sizeable contributions from aggregate forward-scattering effects, the filtering of a *projection* -type system becomes less effective, leading to poor contrast. For this situation, the SNR of an image formed from the object plane may be increased, leading to improved contrast performance for an *one-to-one imaging* -type system.

An interesting prospect for future considerations is the possibility to extend these prescriptions by systematically applying the model to a standard system over a large range of conditions to map the profiles of trends in the trans-illumination signal relevant to specific

#137309 - $15.00 USD Received 2 Nov 2010; revised 21 Dec 2010; accepted 21 Dec 2010; published 18 Jan 2011

imaging problems. Such an approach could be useful in applications ranging from identification of abnormal or precancerous biological tissues to optical drop-sizing techniques for industrial sprays.

The key to mitigating noise and obtaining high quality spatial information from a turbid environment lies in understanding the distribution of photon classes which make up the transmitted signal, and optimally partitioning this distribution to allow photons contributing spatial information from the object of interest to dominate the signal. Careful application of the validated system model discussed here provides a detailed understanding of the trans-illumination signal, enabling accurate quantitative image enhancement in scattering media.

Acknowledgments

Dr. Sedarsky was supported by the Swedish Research Council grant no. 621-2004-5504 and Air Force EOARD grant no. FA8655-06-1-3031. This work was partly performed within the Strategic Research Centre for studies of combustion process, CECOST. The authors were further supported by the Swedish Foundation for Strategic Research (contract A3 05:183).

#137309 - $15.00 USD Received 2 Nov 2010; revised 21 Dec 2010; accepted 21 Dec 2010; published 18 Jan 2011